Chemical Engineering Journal 511 (2025) 162112

Contents lists available at ScienceDirect

Chemical Engineering Journal

journal homepage: www.elsevier.com/locate/cej

Catalytic hydrodenitrogenation, hydrodeoxygenation and hydrogenation reactions of amides, amines, and nitriles over $NiMoS_X/Al_2O_3$ catalysts: Mechanisms, kinetics and transport☆

Matej Žula [a,b], Vid Bačar [a], Michal Mazur [f], Blaž Likozar [a,c,d,e,*]

[a] Department of Catalysis and Chemical Reaction Engineering, National Institute of Chemistry, Hajdrihova 19, SI-1001 Ljubljana, Slovenia
[b] University of Nova Gorica, Vipavska 13, SI-5000 Nova Gorica, Slovenia
[c] Pulp and Paper Institute, Bogišičeva 8, 1000 Ljubljana, Slovenia
[d] Faculty of Polymer Technology, Ozare 19, SI-2380 Slovenj Gradec, Slovenia
[e] Faculty of Chemistry and Chemical Technology, University of Ljubljana, Večna pot 113, SI-1001 Ljubljana, Slovenia
[f] Department of Physical and Macromolecular Chemistry, Faculty of Science, Charles University, Hlavova 8, 12800 Prague, Czech Republic

ARTICLE INFO

Keywords:
Kinetics
Hydrodenitrogenation
Fatty amides
NiMoS
Mechanisms of hydrodenitrogenation

ABSTRACT

The presence and possibility of removal of nitrogen from the bio-based feedstock is a major challenge for efficient use of these sources. Herein, we propose a unique micro-kinetics model which enables the fundamental competing selective mechanism elucidation using sulfided $NiMo/Al_2O_3$, a conventional hydrotreating catalyst. The model was built based on varying temperature and hydrogen pressure. Both, homogeneous and heterogeneous reactions are described in presence and absence of hydrogen with hexadecanamide and hexadecanamine as model compounds. We show that the process can undergo hydrodeoxygenation or hydrodenitrogenation reaction path based on the water/ammonia presence in the reaction mixture. This finding shows that the presence of nitrogen in feedstocks can be manipulated by influencing equilibria. Detailed catalyst characterization and mass transfer analysis support the study. The results represent the foundation for the understanding of catalytic and non-catalytic relationships between the reactants. It was elucidated that the influence of process parameters, including the small molecules presence, can direct of the process selectivity towards amines, dimers, and alkanes.

1. Introduction

The main reason for the rising need for energy nowadays is the growth of the world's population and expansion of the economy [1]. It is estimated that 80 % of all energy comes from fossil fuels [2], accounting for 89 % of the human contribution to global warming. Development and optimization of novel reactions paths enables novel renewable fuels and decreases the energy consumption of chemicals production. Amides are naturally abundant functionality which can on the one hand be upgraded to amines and on the other hand represent a recalcitrant functional group during the hydrotreatment of bio-based feedstocks [3,4].

Beyond the use in fuels, upgrading amides to amines was researched thoroughly using both homogeneous and heterogeneous catalysis [5,6]. It is usually much more economically efficient to use heterogeneous catalysts since they are more stable, require no expensive ligands and are easily separated from the feedstock. Thus, several heterogeneous bifunctional catalysts have been developed [7–12]. These catalysts show excellent performance for secondary and tertiary amides but usually struggle with either yield or selectivity when using primary amides with longer carbon chains [13,14].

Fuels produced from natural sources such as vegetable oils, maize, lignin from lignocellulosic biomass, algae, waste biomass and waste plastics, show promise. They have a high energy and calorific value [15], and can have similar properties to the fossil diesel [16], which means that can be used directly in motor vehicles. The technoeconomic analysis shows that such fuels can be prepared in an economic and sustainable manner [17,18]. The problem is their preparation, with numerous, novel structures in the feedstocks, the process can be slower, the catalyst can get deactivated [19–23]. The reasons for these are often unclear due to the very heterogeneous contents of these feedstocks. The especially difficult part seems to be removal of nitrogen [24].

☆ This article is part of a special issue entitled: 'ISCRE 28' published in Chemical Engineering Journal.
* Corresponding author.

https://doi.org/10.1016/j.cej.2025.162112

Available online 29 March 2025

Table 1
Characterization results of $NiMoS_x$ catalyst.

Characterization method	BET surface	BJH pore diameter	BJH pore volume	TPO-TPR active sites [28]	TPD acid sites [28]
Catalyst	[m^2 g_{cat}^{-1}]	[nm]	[cm^3 g_{cat}^{-1}]	[μmol m^{-2}]	[mmol g_{cat}^{-1}]
$NiMo/\gamma\text{-}Al_2O_3$	135	14	0.535	0.33	1.22

Table 2
Kinetics rate equations with descriptions.

Reaction rate equation	Type of the equation
$r_{1HLY_L} = -k_1 C_{PA,L} C_{H_2O,L}$	NH_3 substitution with H_2O in palmitic amide in liquid
$r_{2KON_L} = -k_2 C_{PK,L} C_{NH_3,L}$	H_2O substitution with NH_3 in palmitic acid in liquid
$r_{3HYL} = -k_3 C_{PA,S} C_{H_2O,S}$	NH_3 substitution with H_2O in of palmitic amide on the surface
$r_{4DOK} = -k_4 C_{PK,S}$	Decarboxylation of palmitic acid
$r_{5HYD} = -k_5 C_{Pdene,S} C_{H_2,S}$	Hydrogenation of pentadecane
$r_{6HDO} = -k_6 C_{PK,S} C_{H_2,S}$	Hydrodeoxygenation of palmitic acid
$r_{7DOK} = -k_7 C_{PAL,S}$	Decarbonylation of hexadecanal
$r_{8HYD} = -k_8 C_{PAL,S} C_{H_2,S}$	Hydrogenation of hexadecanal
$r_{9DHD} = -k_9 C_{HOH,S}$	Dehydration of water from hexadecanol
$r_{10HYD} = -k_{10} C_{Hdene,S} C_{H_2,S}$	Hydrogenation of hexadecene
$r_{11HDO} = -k_{11} C_{PA,S} C_{H_2,S}$	Hydrodeoxygenation of palmitic amide
$r_{12KON_L} = -k_{12} C_{PA,L} C_{PK,L}$	Catalytic dehydration of water from palmitic amide in liquid with palmitic acid as a catalyst
$r_{13KON_L} = -k_{13} C_{PA,L}$	Dehydration of water from palmitic amide in liquid
$r_{14ADC_L} = -k_{14} C_{PN,L} C_{H_2O,L}$	Addition of water on palmitonitril in liquid
$r_{15DHD} = -k_{15} C_{PA,S}$	Dehydration of water from palmitic amide
$r_{16HYD} = -k_{16} C_{PN,S} C_{H_2,S}$	Hydrogenation of palmitic nitrile
$r_{17ELI} = -k_{17} C_{Pamin,S}$	Elimination of hydrogen from hexadecan-1-amine
$r_{18DN} = -k_{18} C_{Pamin,S}^2$	Dimerization of hexadecan-1-amine
$r_{19DN} = -k_{19} C_{Pamin,S} C_{PA,S}$	Dimerization of hexadecan-1-amine and palmitic amide
$r_{20HDN,HDO} = -k_{20} C_{PA,S}^2 C_{H_2,S}$	Formation of a dimer (dihexadecyl amine) from palmitic amide
$r_{21HDN,HDO} = -k_{21} C_{PA,S} C_{H_2,S}$	Formation of a dimer (dihexadecyl amide) from palmitic amide
$r_{22HDO} = -k_{22} C_{DPamid,S} C_{H_2,S}$	Hydrodeoxygenation of *N*-hexadecylpalmitamide
$r_{23DN} = -k_{23} C_{DPamin,S}$	Denitrogenation of dihexandecylamine

With the expansion of the feedstocks to bio-oils the functional such as fatty acids and even fatty amides groups appear in renewable feedstocks but are not present in fossil feedstocks [25]. Nitrogen can be trapped in the biomass in the form of amino acids, amines, or amides. Oxygen is most often present in the form of acids, esters, alcohols, and aldehydes. Beside the natural content of amides in lipid feedstock, the content can increase during biomass processing. Davis et al. [26] showed a reaction between fatty acids and ammonia to fatty amides in the presence of water and ammonia in liquid.

To understand the catalyst activity and the functional group presence, the role of hydrogen and small molecules (NH_3, H_2O, H_2) we have conducted a detailed kinetic analysis using C_{16} model compounds with amide, amine, diamine terminal functional groups in the presence and absence of H_2 gas. The main reaction pathways of interaction were identified as substitution and elimination – condensation reactions. We show that the dehydration is the rate limiting step in formation of dimers. All in all, model combines 25 unique reaction conditions to support mechanistic observations and quantitatively describe temperature and pressure dependences of observed transformations. The work aims to aid both hydrotreatment and amide hydrogenation applications through the first comprehensive quantitative description of homogeneous and heterogeneous interactions of long-chain primary amides.

2. Experimental

2.1. Materials

Palmitic amide (TCI, > 95 %), Palmitic amine (Hexadecan-1-amine) (Sigma-Aldrich, 98 %), dihexadecylamine (Angene International ltd., 98 %), palmitic acid (Acros organics, reagent grade, 98 %), hexadecanol (Sigma-Aldrich, analytical standard), hexadecanal (Biosynth, > 95 %), pentadecane (Fluka, analytical standard), hexadecane (Fluka, analytical standard), dodecane (TCI, > 99 %), hexane (> 98.5 %, Merck), dimethyl disulfide (DMDS) (Sigma–Aldrich, > 99 %), $NiMo/\gamma\text{-}Al_2O_3$, hydrogen (Messer, 5.0), nitrogen (Messer, 5.0), isopropanol (Honeywell, >99.8 %).

2.2. Experimental work

Parr series 5000 Multiple Reactor batch system was used for performing chemical reaction. Unless specified differently, 1 g of palmitic amide, 0.25 g of the sulfided $NiMo/\gamma\text{-}Al_2O_3$ catalyst and 30 g of solvent dodecane were put into the reactor vessel. Reactions were performed in temperature range between 250 and 290 °C and pressure range between

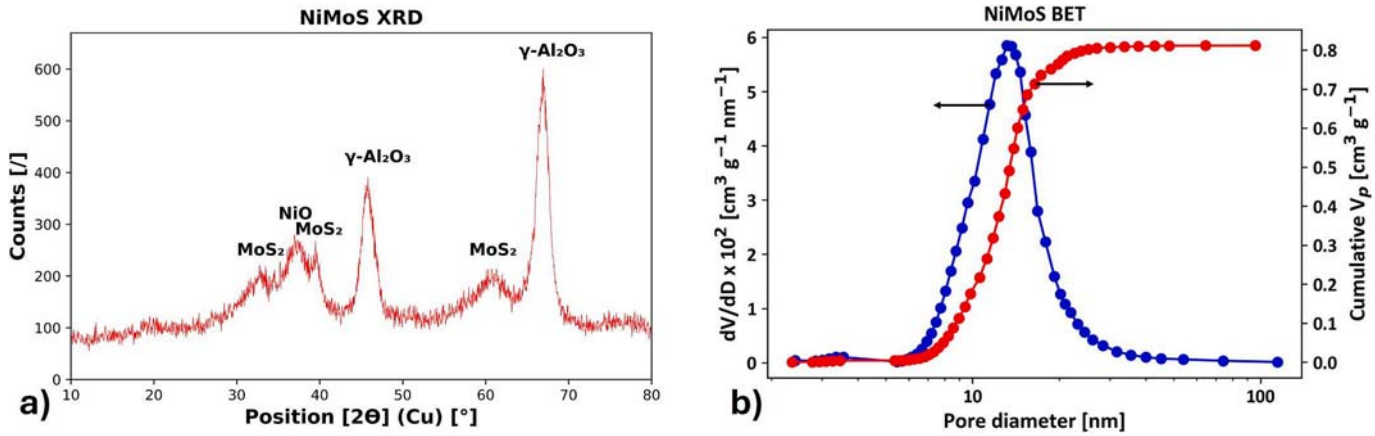

Fig. 1. Analysis of the $NiMoS_X/Al_2O_3$ catalyst: XRD reflections (a) and textural analysis of pore volume and diameter (b).

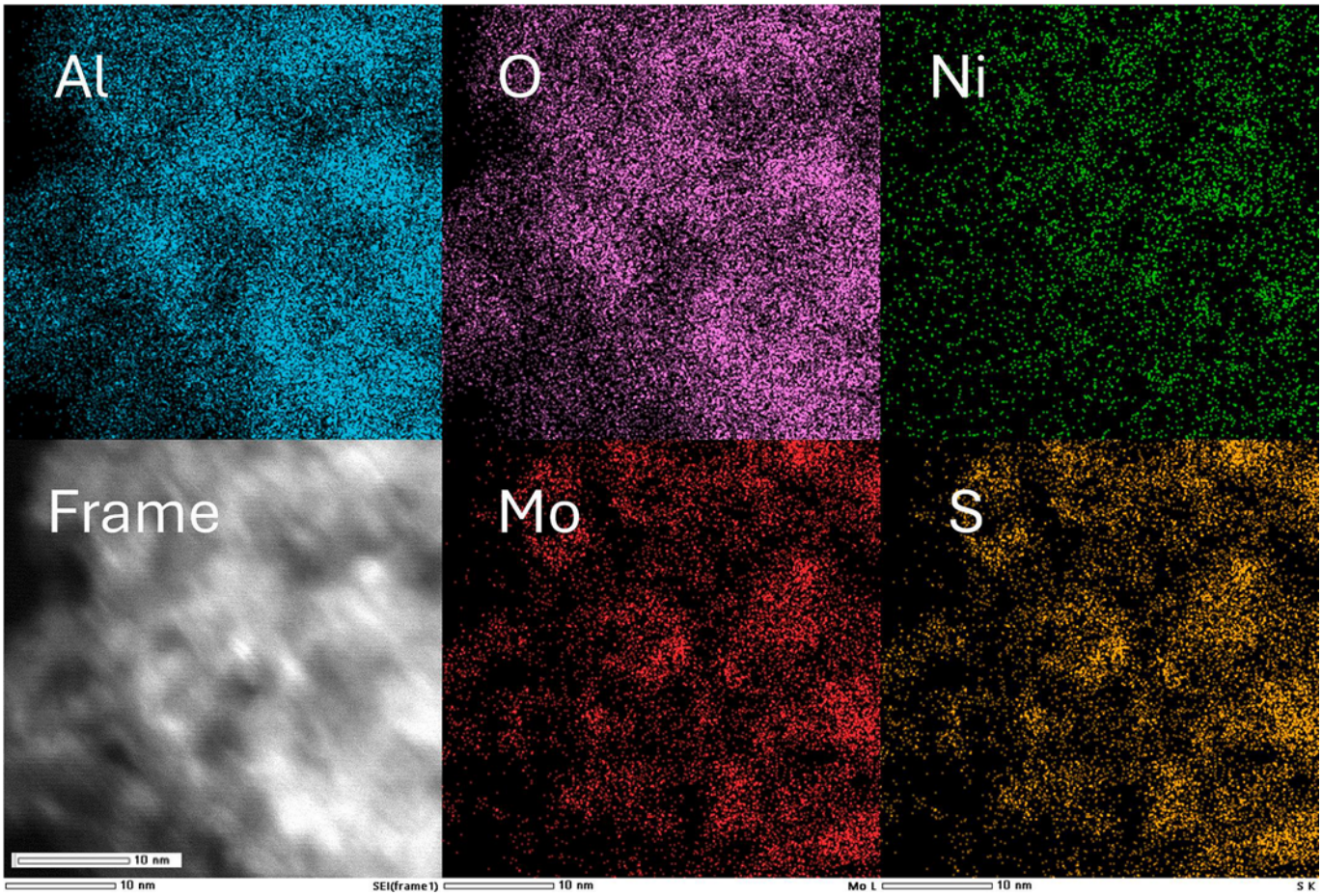

Fig. 2. STEM micrograph of investigated catalyst with corresponding EDS elemental maps of molybdenum (red), sulphur (orange), aluminium (blue), oxygen (violet), and nickel (green). (For interpretation of the references to colour in this figure legend, the reader is referred to the web version of this article.)

30 and 70 bar at 1000 rpm. The experimental errors were determined from the repetition of the middle experiment (270 °C, 50 bar H_2 and 0.25 g_{cat}) and applied as a relative error to other graphs. An average experiment provided 9 samples which were gravimetrically diluted in isopropanol and analysed using GC–MS (GCMS–QP 2010 Ultra, Shimadzu, Kyoto, Japan) equipped with a nonpolar column (Zebron ZB–5MSi, length 60 m, diameter 0.25 mm, film thickness 0.25 μm). The standards were determined using external standards via 5 – point calibration method. Where standards were unattainable the response factor for the most similar molecule was used instead (alkanes for alkenes, palmitic amine for palmitic nitrile and dihexadecylamine for all dimers). More information regarding reaction preparation and sample analysis is available in our previous article [27].

The experimental strategy was firstly to determine the reaction rates without catalyst for which three experiments were done with palmitic amide at different temperatures. To further elaborate the impact of palmitic acid on equilibrium the mixture of palmitic acid and palmitic amide was tested. Catalyst was then added to the mixture in N_2 atmosphere to describe the dehydration reactions and separate them from any hydrogenolysis reactions. Finally, the hydrogen was added to the mixture to show impact of hydrogenolysis and hydrogenation on the reaction rates. To describe the impact of pressure, the experiments were done in at three different initial hydrogen pressures (30, 50 and 70 bar). Due to a significant number of reactions palmitic amine was tested under both H2 and N2 atmosphere. Dihexadecyl amine was used in a single reaction due to quantitative restraints. Lastly, the mixtures between palmitic amide and palmitic acid were used to increase the confidence in the obtained parameters and to observe the influence of the presence of palmitic amide on the HDO of palmitic acid, which is an commonly described reaction.

2.3. Catalyst activation and characterization

The used catalyst is commercial 3 wt% Ni 15 wt% Mo γ-Al_2O_3. The catalyst particles were crushed below 100 μm to ensure no internal mass transfer impact and ensure efficient heat exchange with the liquid phase to minimize the impact of exothermicity on the reaction rate. The catalyst activation method and characterization (TPD, TPR-TPO) are described in our previous works [27,28]. Briefly, the activation process included drying at 200 °C over night, dried catalyst was sulfided in the batch reactor using 15 g of the catalyst, 3 g of dimethyl disulfide (DMDS) and 20 mL of hexane at 350 °C for 90 min at the initial H_2 pressure of 25 bars. Concentration of accessible active phase was determined by consecutive H2-TPR, O2-TPO and H2-TPR cycles (Temperature programmed reduction/oxidation). 0.05 g of catalyst was heated-up (10 K min^{-1}) starting at 50 °C to 700 °C under a flow of 10 % H_2/He or 10 % O_2/He for TPR and TPO step. The uptake of H_2 or O_2 was measured by a thermal-conductivity detector. X-ray diffraction (XRD), N_2 physisorption, and Scanning transmission electron microscopy (STEM) analysis were done for the purpose of this work to both show and understand the catalyst structure. Results of the characterization are presented in Table 1.

XRD patterns were characterized using PW3040/60 X'Pert PRO MPD diffractometer at 35 kV and 45 mA with Cu Kα radiation source (λ = 0.154056 nm) in the 2θ range from 10° to 80° and using JCPDS database for reference. N_2 physisorption using Brunauer-Emmett-Teller (BET) method was analysed with ASAP™ 2020. The sample was degassed at 453 K and 0.40 Pa for 2 h before the analysis.

Table 3
Kinetic results.

Kinetic parameters (T_r = 543 K)			
Reaction	k_i [min^{-1}]	Ea [kJ mol^{-1}]	Description
(1 (1) HDN $_L$	13.2 ± 1.2 [a]	7×10^{-2} ± 20	Hydrogenation of palmitic amide in liquid
(2) KON $_L$	214 ± 14 [a]	9 ± 10	Condensation of water from palmitic acid in liquid
(3) HDN	0.47 ± 0.09	96 ± 12.3	Hydrodenitrogenation of palmitic amide
(4) DOK	0.29 ± 0.05	114 ± 24	Decarboxylation of palmitic acid
(5) HYD	5.5 ± 4 × 10^3	43 ± 32	Hydrogenation of pentadecane
(6) HDO	3.1 ± 0.3 × 10^3	142 ± 40	Hydrodeoxygenation of palmitic acid
(7) DOK	75 ± 55	35 ± 33	Decarboxylation of hexadecanal
(8) HYD	4.1 ± 2.1 × 10^5	22 ± 16	Hydrogenation of hexadecanal
(9) KON	2.9 ± 2 × 10^3	22 ± 17	Dehydration of water from hexadecanol
(10) HYD	1 ± 0.5 × 10^4	1 ± 25	Hydrogenation of hexadecene
(11) HDO	360 ± 23	248 ± 43	Hydrodeoxygenation of palmitic amide
(12) KON $_{L,\ kat}$	5.0 ± 0.5 × 10^{-2b}	110 ± 23	Catalytic condensation of water from palmitic amide in liquid with palmitic acid
(13) KON $_L$	3.3 ± 0.1 × 10^{-4} [a]	25 ± 1	Dehydration of water from palmitic amide in liquid
(14) ADC $_L$	2.8 ± 0.1 [a]	13 ± 2	Addition of water on palmitonitril in liquid
(15) KON	0.6 ± 0.2	154 ± 76	Dehydration of water from palmitic amide
(16) HYD	663 ± 196	192 ± 56	Hydrogenation of palmitic nitrile
(17) ELI	3.6 ± 2.8 × 10^{-4}	17 ± 15	Elimination of hydrogen from hexadecan-1-amine
(18) DN	8.6 ± 0.9 × 10^{4c}	163 ± 22	Denitrogenation of hexadecan-1-amine
(19) DN	1.2 ± 0.7 × 10^{5c}	< 0.05 ± 20	Dimerization of hexadecan-1-amine and palmitic amide
(20) HDN HDO	3.5 ± 2.1 × 10^{8c}	146 ± 73	Dimerization of palmitic amide to Dihexadecyl amine
(21) HDN HDO	1.5 ± 0.6 × 10^3	112 ± 64	Dimerization of palmitic amide to Hexadecylpalmitamide
(22) HDO	685 ± 419	153 ± 81	Hydrodeoxygenation of *N*-hexadecylpalmitamide
(23) DN	3.7 ± 1.8	43 ± 26	Denitrogenation of dihexandecylamine

Reactions with indices have customised units: [a] [L min^{-1}], [b] [L mol^{-1} min^{-1}], [c] [mol^{-1} min^{-1}].

STEM measurements were performed using JEOL JEM NEOARM-200F microscope equipped with Schottky type field-emission gun operating at 200 kV. Samples were prepared by direct deposition of the powder on copper holey carbon TEM grids (300 square mesh, EMR, United Kingdom). Images were collected in scanning mode using a JEOL annular dark-field (ADF) and bright-field (ABF) detectors. Energy dispersive X-ray spectroscopy (EDS) elemental distribution maps were acquired using a JEOL JED-2300 energy dispersive X-ray analyser.

The resulting STEM data were used to estimate the extent of Ni and Mo sulfidation as well as the degree of NiMo alloying on the catalyst. By using the OpenCV2 module, we converted the pixels from the STEM images into Python data. The STEM image was segmented into a 2D grid, with each pixel assigned specific coordinates and RGB values. Given that the background was black, we applied an algorithm described and then applied Eq. 1 (an example for sulfur coverage on molybdenum) to determine the coverage. We analysed this data and identified the overlap between the elements using the numpy package in Python. By comparing data between the individual elements, we established the overlap between them. Furthermore, with Monte Carlo method we checked the degree of random coverage.

$$coverage\ of\ \frac{Ni}{Mo} = \frac{number\ of\ same\ site\ (Ni\ and\ Mo)}{number\ of\ Mo\ sites} 100\,\% \tag{1}$$

3. Modelling

For the compounds which are present in gas and liquid phase the equilibrium was determined by using program Aspen®. The correlation was described for the pressure range up to 70 bar, for the temperatures between 200 and 300 °C, the liquid and gas phase were simulated as in reactor – liquid would include above 95 wt% dodecane while gas phase would include between 10 and 80 bar of hydrogen. Obtained data were described via regression resulting in Eq. (2), the uppercase letters from A to L (except K) present constants for gas–liquid compounds.

$$K = A + Bx_{C_{12}} + Cx_{NH_3} + Dx_{H_2O} + Ey_{H_2} + Fy_{C_{12}} + Gy_{NH_3} + \\ +H(T - T_r) + I(p - p_r) + J(T - T_r)^2 + L(p - p_r)^2 \# \tag{2}$$

The gas–liquid mass transport of hydrogen was described with Henry's constant based on the experimental work of Gao et. al.[33], the kinetics of transport were described with the Eq. (3).

$$\frac{dn}{dt} = k_L \times a \times \left(\frac{p}{He} \times \frac{M_{DD}}{\rho_{DD}} - C_{H_2L}\right) \# \tag{3}$$

The rest of transport phenomena are explained in detail in our previous work [27].

The modelling was done step by step from gas phase to the catalyst surface. Surface chemistry is described by Langmuir's classical theory, reaction rate constants follow the Arrhenius relation and chemical reaction equations are in elementary forms.

Reactions follow first order reaction Eq. (4) or pseudo first order reactions Eq. (5). Second order reactions Eq. (6) are formation of dimers R18, R19 and R20 and catalytic reaction R12 from palmitic amide to palmitic nitrile. Liquid phase equations are expressed as Eq. (7) and (8). All the kinetics rate equation are presented in Table 2.

$$r_i = -kC_{a,s} \# \tag{4}$$

$$r_i = -kC_{a,s}C_{H_2,s} \# \tag{5}$$

$$r_i = -kC_{a,s}C_{b,s} \# \tag{6}$$

$$r_i = -kC_aC_b \# \tag{7}$$

$$r_i = -kC_a \# \tag{8}$$

Hydrogen was presumed to adsorb as molecule (neglected hydrogen splitting) independently while all other species take one active site, but dimers dihexadecylamine and *N*–hexadecylpalmitamide are considered to take two spots. Due to the lack of data the adsorption and desorption constants are same for all compounds except hydrogen. The adsorption values were fitted to the experimental data. The starting approximations were considered in a way that has enabled the full coverage of the catalytic sites at most concentrations which is in line with the literature on fatty acids HDO [29–31]. The adsorption reactions would take the form of Eq. (9) while the desorption would take the form of Eq. (10).

$$r_{i,ads} = -k_{ads}C_{a,L}\frac{N_{Freesites}}{N_{sites}} \# \tag{9}$$

$$r_{i,des} = -kC_{a,s} \# \tag{10}$$

The rate and adsorption constants were calculated using the least square approximation method using the Nedler-Mead and Levenberg-Marquardt algorithms to determine the kinetic parameters. In Eq. (11) the *EXP*, *nS* and *nC* represent the different experiments, samples and compounds respectively. Note that the concentrations in the Eq. (11) are liquid phase.

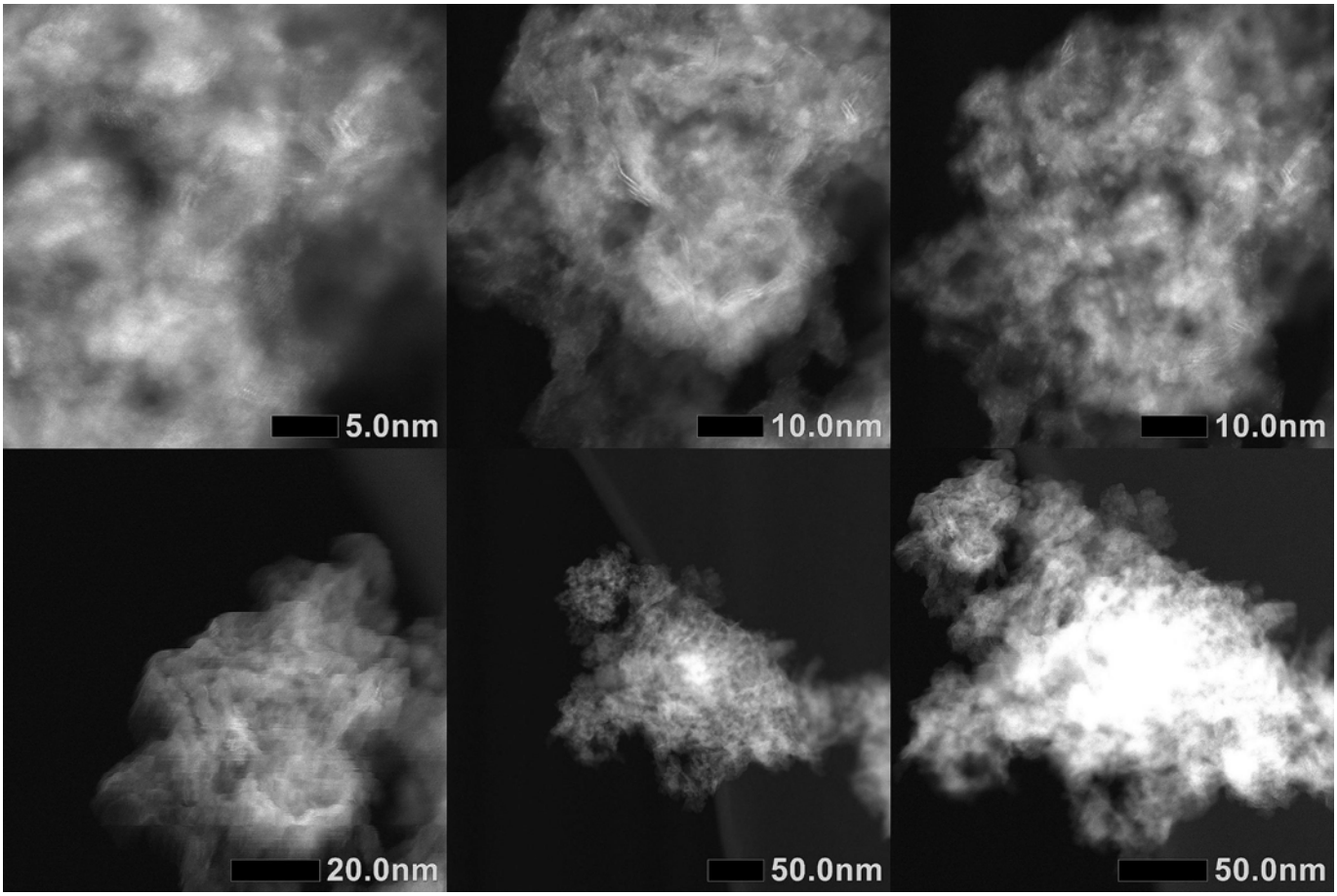

Fig. 3. STEM images of NiMo/γ-Al_2O_3 catalyst taken at different magnifications.

$$f(k_n, Ea_n) = \sum_{j=1}^{EXP}\sum_{i=1}^{nS}\sum_{C=1}^{nC}\left(C_{j,i}^{exp} - C_{j,i}^{mod}\right)^2 \# \quad (11)$$

The 95 % confidence intervals were calculated using "trust-region-reflective" algorithm.

The elimination of species is calculated with following equation:

$$Nelimination = \frac{n_{N,products}}{n_{N,reactants}} \times 100\% \# \quad (12)$$

$$Oelimination = \frac{n_{O,products}}{n_{O,reactants}} \times 100\% \# \quad (13)$$

For comparison of the obtained results with the results from the literature the process intensity was recalculated to holding time τ [min]

$$\tau = \frac{m_{cat}t}{m_A} \# \quad (14)$$

where m_{cat} [g] is mass of the catalyst, t [min] time, and m_A [g] mass of the palmitic amide if not stated differently.

To describe the mass transport of the molecules between the gas and the liquid the Eq. (15) was solved based on the experimental solution for the mass transport in the dead-end reactions. While the solution was implemented for the transport of H_2, the same coefficient was used for the transport of NH_3 and H_2O.

$$\frac{k_L \times a}{V_L \times D_{H_2,DD}(T)} = 1.5 \times 10^{-4} \times Re^{1.45} \times Sc^{0.5} \times We^{0.5} \# \quad (15)$$

Area was estimated as the curved surface of a cone with $r = 1.7 \times 10^{-2}$ m and $L = 5 \times 10^{-2}$ m which was experimentally measured and is specific for Parr 5000 reactor size.

The diffusivity of hydrogen in dodecane ($D_{H_2,DD}$) was obtained from the work by Matthews et. al. [32] and viscosity (μ) and density (ρ_{DD}) of dodecane were obtained from the work of Koller et. al. [33], Reynolds, Schmidt and Weber numbers were obtained by Eqs. 16–18.

$$Re = \frac{\rho_{DD} \times N \times d^2}{\mu} \# \quad (16)$$

$$Sc = \frac{\mu}{\rho_{DD} \times D_{H_2,DD}(T)} \# \quad (17)$$

$$We = \frac{N^2 d^3 \rho_{DD}}{\sigma} \# \quad (18)$$

4. Results and discussion

4.1. Catalyst characterization results

XRD was done to describe the catalyst structure (Fig. 1). Particles are amorphous which is seen by wide peaks of MoS_2 and NiO species. Ni is in oxide form because of exposure to the atmosphere but is expected to reduce during the initial reaction stages. Results agree with the work of Del Rio et. al. [34].

BET analysis showed similar results as the data from the literature [35].

From STEM-EDS analysis three sets of pictures (one set is shown on Fig. 2) were obtained and analysed. The average results of the three images are presented in Table S1. It is showed that molybdenum and sulphur are always linked together. Mo and Ni are equally represented all over the surface. The coverage between Mo and S is close to 98 %. Overlap between Mo and Ni indicates nickel is randomly distributed

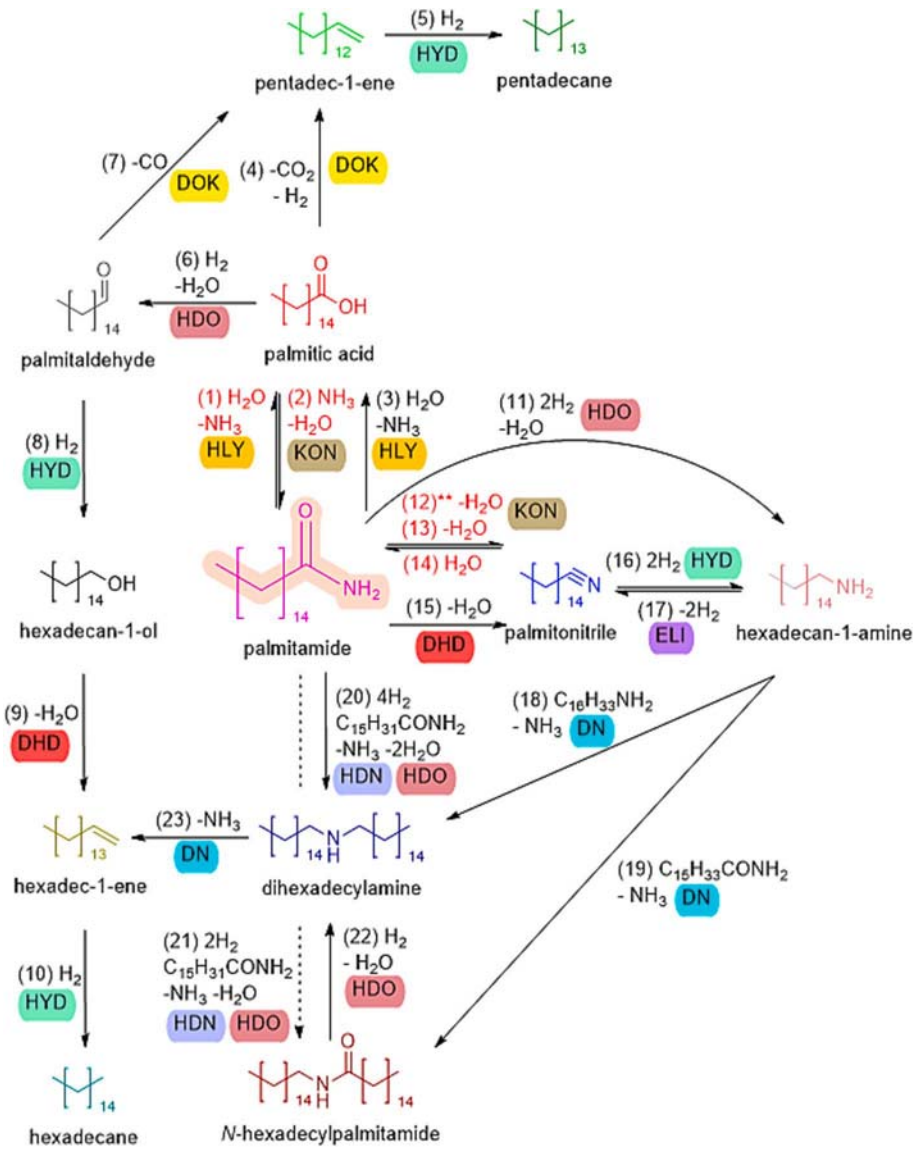

Fig. 4. Reaction scheme with mechanisms and chemical reaction indexes. **Reaction is additionally catalysed by palmitic acid. Legend: Hydrogenation – HYD, DOK – Decarbonization, HDO – Hydrodeoxygenation, HDN – Hydrodenitrogenation, KON – condensation, ELI – elimination, DN – denitrogenation and ADC – addition, DHD – dehydration.

Table 4
Coefficients for empirical equation (2).

	A	B	C	D	E	F	G	H	I $\times10^{-3}$	J $\times10^{-2}$	L $\times10^{-5}$
H_2	−163	139	215	97.7	25.4	4626	41.2	−5.26	1.66	−3.91	1.31
NH_3	−16.3	−6.03	−17.0	−1.87	22.3	227	24.2	−0.13	−0.52	−0.14	−0.87
H_2O	−7.18	6.36	7.27	5.12	0.84	68.2	−1.61	−0.066	0.22	−0.058	0.36
C_{12} [$\times10^{-2}$]	−0.65	2.34	2.65	2.46	−1.65	98.2	−1.18	0.0021	−0.016	0.00086	−0.094

over the surface of the catalyst with comparison to molybdenum. The Monte Carlo (M. C.) analysis agrees with the findings since the results are within the 15 % difference among each other. Since nickel is free on the catalyst surface, it is likely that it not only acts as a promoter of MoS edges, but there might be a significant amount of Ni sites which are responsible for hydrogen activation. The MoS_2 structures can be observed on Fig. 3.

4.2. Reaction scheme

With 25 experiments we designed a reaction scheme with 23 chemical reactions. Reaction scheme (Fig. 4) can be divided into two main pathways. First pathway called the oxygen path happens when NH_3 in amide is substituted with water to palmitic acid as a main compound. Such mechanisms were previously described in detail [30,34,36,37]. The other side, the nitrogen path, starts with palmitic amide and goes through its main intermediate palmitic nitrile. The

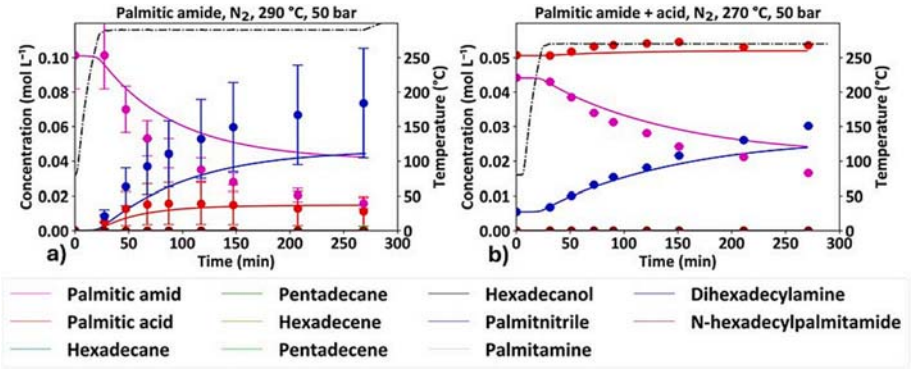

Fig. 5. Reaction of palmitic amide in nitrogen (a). Reaction between palmitic amide and palmitic acid in nitrogen (b).

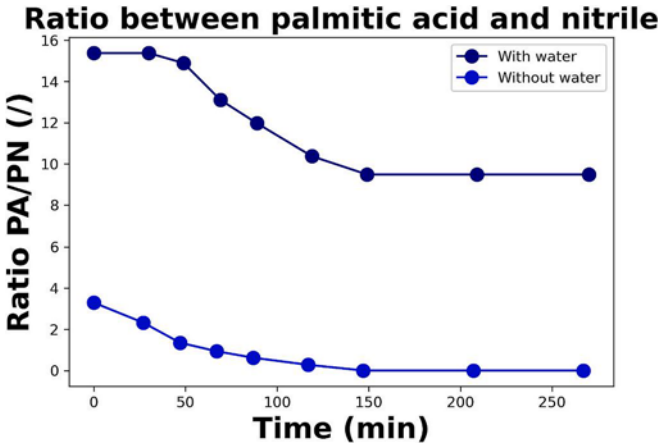

Fig. 6. Ratio of palmitic acid to palmitic nitrile during the reaction is dependent on water.

Table 5
Literature overview of nitrogen elimination.

Catalyst	Pt/ ZrO_2	Ni/ C	NiMo/ γ-Al_2O_3	NiMo/ γ-Al_2O_3
Nitrogen elimination [%]	45	32.2	92	22.5
Holding time [g_{cat} h g^{-1}_{amida}]	0.37	1.96	8	2
Mass of amide / biomass [g]	0.054	40	4	4
T [°C]	300	350	350/400*	330
m_{cat} [g]	0.02	8	2	2
Pressure [bar]	80	68.9	80	80
Time [h]	1	10	4/4	4
Source	[48]	[49]	[50]	[50]

* Reaction was done in two steps at different temperature and time.

nitrogen path was supported by the results of Verkama et al. [38] and developed through the results of this work for the purpose of quantitative description of the process. The reaction starts via dehydration of palmitic amide, during the dehydration the protonated molecule can stabilize to palmitic nitrile or through the formation of the dimer with molecules in the immediate proximity. The palmitic nitrile can be hydrogenated to amine with imine not being present in the liquid phase. Hexadecane is formed mainly through hexadecene path indicating C-N bond cracking in palmitic amine and dihexadecyl amine. The results agree with the work of Prins [39] where he shows that the bond between aliphatic chain and amine group is the most labile. However, at this point it seems that the main reaction pathway of the splitting is not hydrogenolysis but the NH_3 removal and formation of unsaturated alkene (see the Fig. 7 denitrogenation of palmitic amine under H_2 and N_2 atmosphere). Reactions coloured in red take place in liquid.

4.3. Kinetic parameters

They system includes all 11 compounds and 23 chemical reactions which react through 8 different types of reactions. The kinetic results can be found in Table 4. The main reaction pathways include hydrodenitrogenation, hydrodeoxygenation and dehydration which are responsible for formation of intermediates, hydrogenation than converts intermediates to products. Some side reactions of addition, elimination, denitrogenation and decarbonization are present as well. The process can thus be split in multiple parts that happen subsequently to some degree. Firstly, the palmitic amide undergoes either the dehydration to the palmitic nitrile (R12, R13, R15) or the NH_2 group is substituted with OH group forming palmitic acid (R1 and R3). The process is less dependent on temperature as can be observed from low activation energies (0–30 KJ mol^{-1}). The selectivity of the process is determined by the presence of water as can be concluded by the reaction rate expressions in Table 2. During the dehydration of palmitic amide presumably the protonated palmitic nitrile forms which can stabilize or form the dimers with species present on the catalyst forming dimers such as dihexadecyl amine, dihexadecyl amide (R18, R19, R20, R21). The process of dimer formation includes the removal of nitrogen from the carbon chains which is why temperature dependence and thus energies of activation are higher (>100 KJ mol^{-1}). The complete removal of nitrogen is achieved via denitrogenation which is removal of nitrogen in the form of NH_3 from dihexadecyl amine and formation of two unsaturated chains (hexadecene) (R23). Alternatively, the process can undergo the hydrodeoxygenation pathway when fatty acid is formed which is significantly faster than hydrodenitrogenation (R4-R10, see our previous work on hydrodeoxygenation of palmitic acid at the same acid and catalyst loading [36]).

4.4. Water and ammonia equilibrium

Water and ammonia participation in the reaction and their effect on the equilibrium between palmitic amide, palmitic acid and palmitic nitrile is demonstrated by the reactions of palmitic amide and the reaction of palmitic amide and palmitic acid in the nitrogen atmosphere. No other products are formed during the reactions. The addition of water shifts the equilibrium between the species, resulting in more palmitic acid being formed compared to palmitic nitrile. The system is in equilibrium.

$$H_2O + C_{15}H_{31}CONH_2 \leftrightarrow NH_3 + C_{15}C_{31}COOH\# \quad (19)$$

Ratio between the species is shown on the graph 5 and it was calculated via Eq. (19).

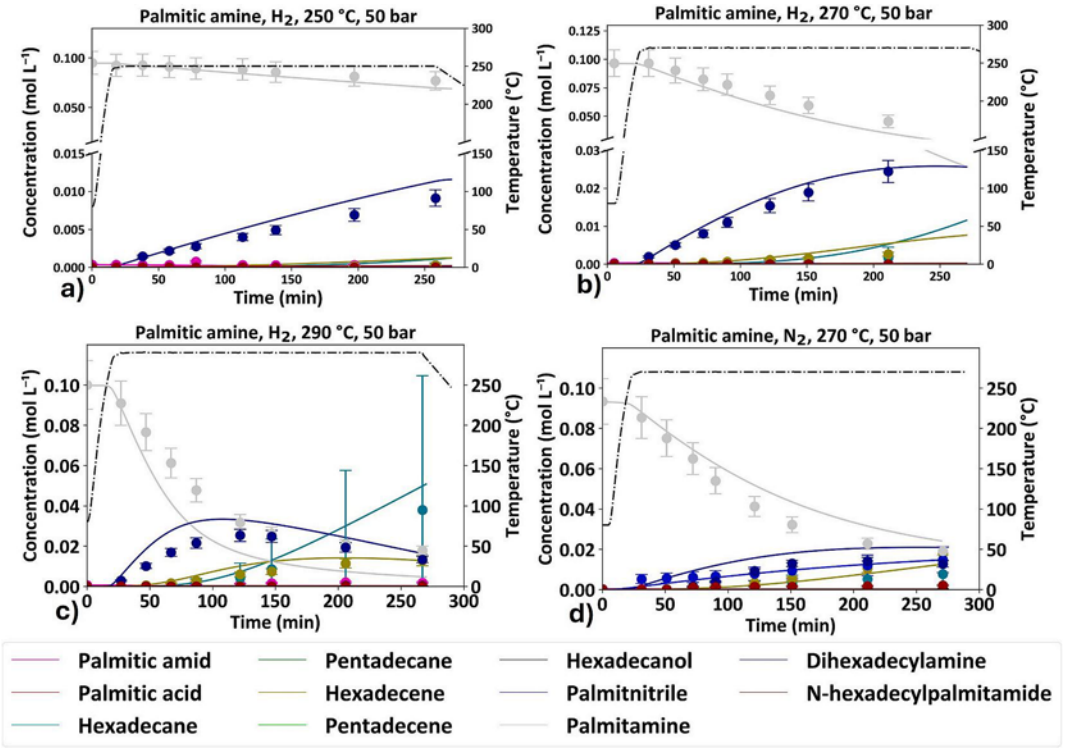

Fig. 7. Palmitic amine reactions at different conditions.

$$Ratio\frac{PA}{PN} = \frac{C_{palmiticacid}}{C_{plamitonitrile}}\# \quad (20)$$

Reactions in nitrogen atmosphere are presented on Fig. 5. Reactions do not have any other products but palmitic nitrile and palmitic acid. The large degree of observed dehydration agrees with the work of Ravn and Rezayee [40] who have shown that acidic catalysts prioritize the removal of oxygen through water. The reaction of palmitic amide dehydration to palmitic nitrile forms water which then pushes the equilibrium in Eq. (18) to the right forming palmitic acid and ammonia. On the other hand, in complex feedstocks the amine groups and fatty acid functional groups can form recalcitrant secondary amides which are hard to defunctionalize [41–43]. Addition of water also shifts the equilibrium between the species and as a result it is seen that more palmitic acid is formed compared to palmitic nitrile (See Fig. 6). Reaction (Fig. 6) was done with 0.032 mol of water or 8 times more moles of water then the palmitic amide at 290 °C and 50 bar of H_2.

Once the relations between discussed compounds were settled, we had to determine gas–liquid equilibrium for water and ammonia. To do so data library from Aspen® was used. Data were transformed into empirical equation Eq. (2) for system hydrogen – dodecane – ammonia – water via regression. Equation was used for all compounds but hydrogen because we believe that mass transfer equations better describe the behaviour of hydrogen. The results can be found in Table 5.

4.5. Palmitic amine reactions

To understand the investigated system, we have firstly performed the reactions under nitrogen where the equilibrium between amine in nitrile was determined (backwards reaction rate) as well as formation of dihexadecylamine. Small amount of product hexadecene is also present. The equimolar reaction with palmitic amine and amide under N_2 shows the formation of *N*–hexadecylpalmitamide. The result is in the agreement with the literature [44]. Reactions with hydrogen further hydrogenated hexadecene to saturated form. The results are presented on Fig. 7.

Reactions are highly temperature dependent due to the high activation energy of formation of dihexadecylamine ($Ea_{18,\ DN}$ = 163 kJ mol^{-1}). The value is comparable to the hydrodenitrogenation activation energies in the work of Nguyen et. al. [45,46].

Activation energy of breaking dimer ($Ea_{23,\ DN}$ = 42.8 kJ mol^{-1}) is low compared to Zhu's et al. [47] hydrodenitrogenation reaction of tercial amine (Ea_{Zhu} = 146 kJ mol^{-1}). This could be due to the spherical obstacles of additional compound on the nitrogen atom, as well the different reaction mechanism. Note as well that palmitic amine, dihexadecyl amine and hexadecene are in equilibrium (see Fig. 10) which is neglected in the model and can be the reason for a lower apparent activation energy of deamination. It should however be considered in the future works. Unlike other works this work shows that hydrogen might not be necessary for the hydrogen C-N bond breaking and the mechanism would likely resemble dehydration mechanism. Importantly, in other works the researchers worked largely with quinolone [45] and pyridine which in nitrogen atmosphere would rapidly deactivate the catalyst via double bond – aromatic ring polymerization to coke [19]. Linear amines hydrodeamination differs from the aromatic amines is in the formation of dimers – secondary amines which are significantly more present in linear amines, the concentrations up to 30 % can be found even at such low concentrations of model compound. The reason for the lack of dimers is unclear – it could be due to steric hindrance of the cyclic tail, lower selectivity at higher temperatures or lower working temperatures on the GC-FID.

Activation energy of hexadecene is relatively low ($Ea_{10,\ HYD}$ = 0.98 kJ mol^{-1}) in comparison with our previous work (Ea = 29 kJ mol^{-1}) [27] using same catalyst. Moreover, in both cases activation energies are low showing weak dependence of hydrogenation reactions on temperature. The relatively high difference might be due to worse fits and/or different interaction between catalyst hydrogenation activity and nitrogen compounds presence.

Reactions with palmitic amine showed low dependence on the H_2 pressure (See Figure SI 4). No reaction was observed in the absence of catalyst. Model expects hexadecane as the only product after 6 h of reactions at 290 °C.

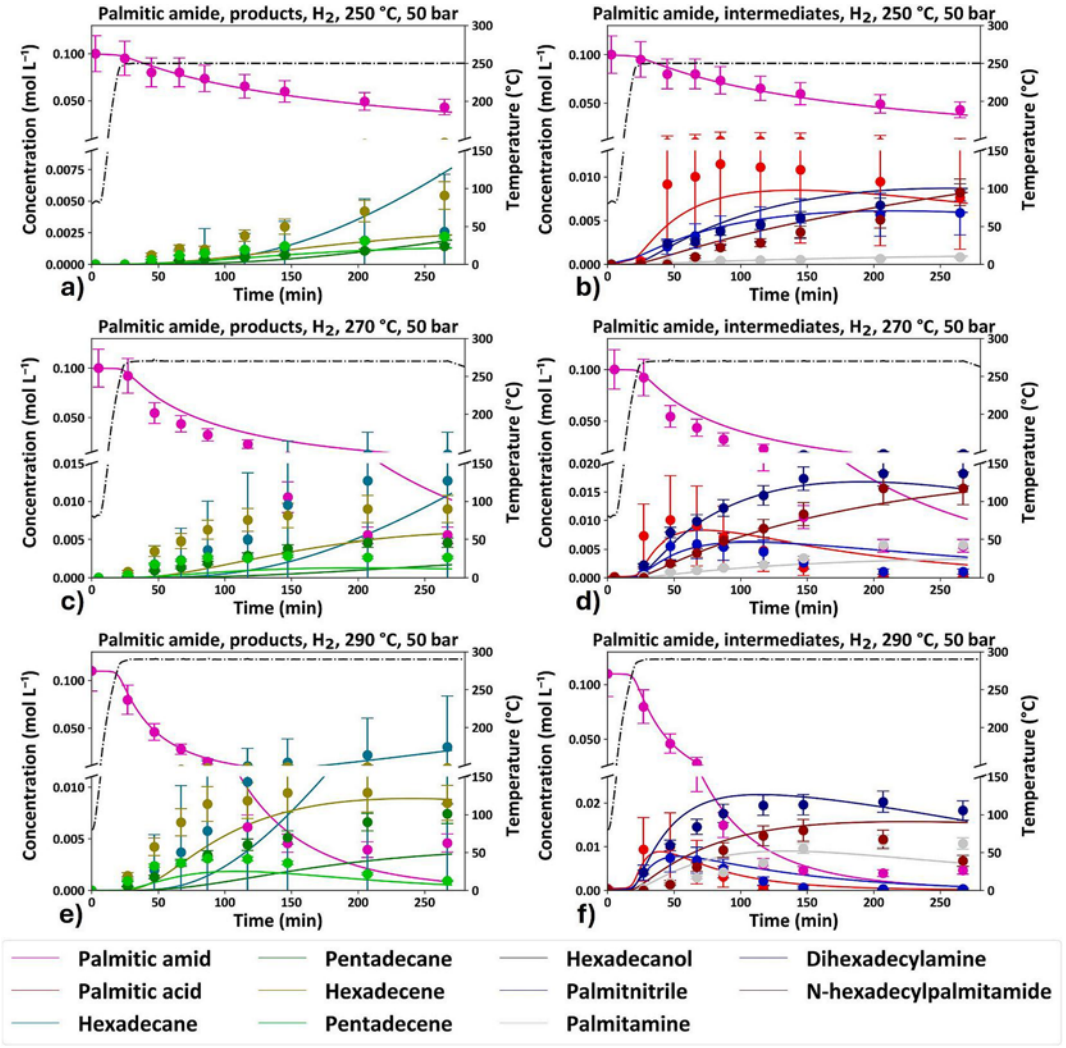

Fig. 8. Main model reaction of palmitic amide at different temperatures.

4.6. Palmitic amide reactions

Homogeneous reactions were done at temperatures between 270 and 290 °C at 50 bar of H_2 pressure (See Figures SI5 and SI6). In this way the liquid reaction rates (forwards and backwards) and activation energies were determined separately from the catalytic reactions. The model predicts additional homogeneous catalytic reactions with H^+ ions from palmitic acid as a catalyst and palmitic amide to palmitic nitrile (R12).

Due to the complexity of the system all but two reverse reactions in liquid (R2 for palmitic acid/amid and R14 for palmitic amid/nitril) were neglected. NiMoS increases the rates of palmitic amide conversion but the reaction in liquid is still more important. It leads the system with reaction rate constant of reaction R1 (HDN_L) with 13.16 L min^{-1} compared to the dehydration on the catalyst surface describe with reaction constant R3 (HDN) with 0.466 min^{-1}.

The reactions are heavily dependent on temperature (Fig. 8) due to the high activation energy of hydrodeoxygenation of palmitic amide to palmitic amine (hexadecan-1-amine) (Ea_{11} = 248 KJ mol^{-1}), denitrogenation of palmitic amine to dihexadecyl amine (Ea_{18} 163 KJ mol^{-1}), dehydration of water from palmitic amide (Ea_{15} = 154 KJ mol^{-1}), hydrogenation of palmitic nitrile to amine (Ea_{16} = 192 KJ mol^{-1}) and other reactions with high activation energy. All reactions of palmitic amide on the catalyst have activation energy near 100 KJ mol^{-1} or higher. Therefore, the system is more selective from palmitic amide towards palmitic acid at low temperatures, because reaction in liquid (R1) has low activation energy (Ea_1 = 76.4 J mol^{-1}). At high temperatures the reactions can overcome the activation barrier which results is higher selectivity of hexadecane. Activation energy of hydrodeoxygenation of palmitic acid to hexadecanal (Ea_6 = 142 kJ mol^{-1}) is higher than in our previous work [27] (Ea = 93 kJ mol^{-1}) and lower than in literature [30]. It is hard to speculate on the reasons for it. It could be due to adsorption selectivity at different temperatures since the coverage is a strongly related to temperature and several new species are introduced in this system. On the other hand, it could be due to numerical inaccuracy considering negligent concentrations of fatty aldehyde and low concentrations of hexadecanol are detected in the system.

The increase in pressure leads to a higher reactant conversion (Fig. 9), which can be explained by the higher solubility of hydrogen in the liquid phase and consequently higher hydrogen coverage of the catalyst. In addition, the equilibrium between the gas phase and the liquid phase of water and ammonia gases is affected by the higher pressure. Thermodynamically, this means that the concentration of these gases should increase in the liquid phase. At higher pressures, the palmitic acid peak is much lower, even though the palmitic nitrile peak is higher, which is the source of water for acid formation. From this we conclude that the gases are far from thermodynamic equilibrium and the effect of pressure on mass transport is negligible. At higher pressure, the number of products increases, and the number of intermediates decreases. The reason therefore lies in the solubility of hydrogen.

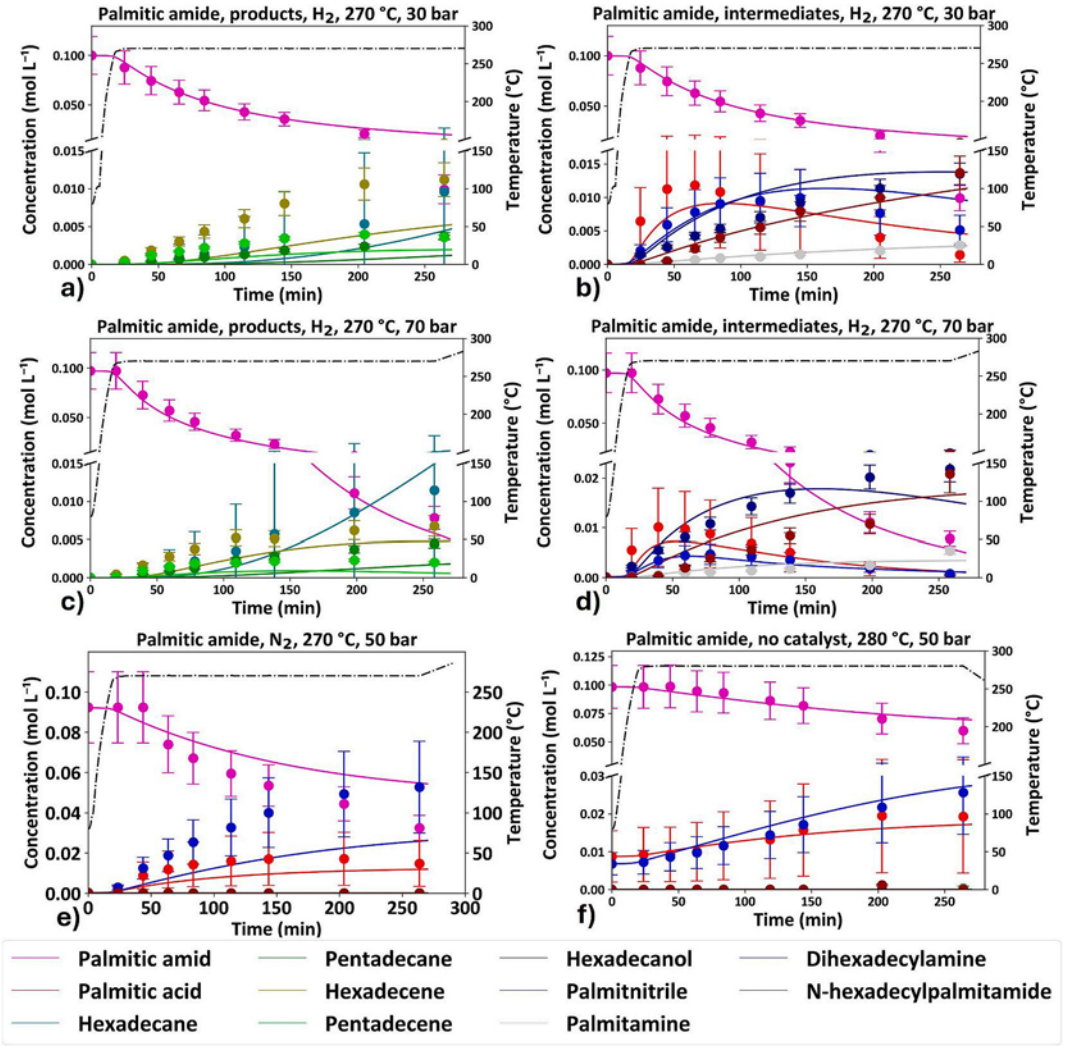

Fig. 9. Main model reaction of palmitic amide at different pressures (a, b, c, d), atmosphere (e) and without catalyst (f).

4.7. Other reactions

Reactions including two species and a reaction with dihexadecyl amine were performed to improve the quality of the model and to show the reaction pathways. The reaction between palmitic amide and palmitic amine (Fig. 10a) in nitrogen atmosphere shows the formation of *N*–hexadecylpalmitamide. In experiment with dihexadecylamine as a reactant high amount of hexadecane is formed quite selectively. The reversible formation of palmitic amine is observed however the reverse reaction is slow compared to other rates and it could not be properly described. The data from this experiment are normalized. Finally, a series of experiments were made in hydrogen including equimolar concentration of palmitic amide and palmitic acid (Fig. 10c and 10d, see also Figure SI7). The data from experiments are normalized. More experiments are provided in supplementary information.

4.8. Elimination of nitrogen and oxygen

Table 6 shows a brief overview of nitrogen elimination from biomass or palmitic amide as a model compound. Note that biomass can contain different functional groups such as aromatic amines and cyclic amines.

Curves of elimination follow the same shape and have limit at 66.9 % (290 °C and 50 bar) or 70.9 % (270 °C and 70 bar) for nitrogen and 75.7 % for oxygen (290 °C and 50 bar). The reason for limitation of elimination process is in high activation energies ($Ea_{22} = 153$ kJ mol^{-1}) and low reaction rate constants ($k_{23} = 3.666$ min^{-1}) of dimers that occur is system. The result is probably the first plateau to be reached in this temperature range. The effect of pressure and hydrogen on removal is shown, suggesting that pressure can make the process more efficient. To compare the results with Verkama et al. [38,48] the data was converted to holding time.

At holding time 0.37 g_{cat} h g_{amide}^{-1} Verkama et al. got around 45 % elimination of nitrogen and around 80 % elimination of oxygen (Pt/TiO_2 catalyst, 80 bar H_2, 300 °C) [48] which is equivalent to results at 120 min for this system. The removal of N on NiMoS is with 55 % for 10 % higher than on Pt/TiO_2 at 10 °C lower temperature. For same catalyst and conditions, they have reached 80 % or reduction of oxygen in the system which is for 20 % higher than NiMoS. Comparing with Pt catalysts NiMoS catalyses more dimers formation which block the oxygen pathway and trap oxygen into less reactive species. On Pt they report only 20 % of dihexadecylamine in comparison to more than 30 % for NiMoS experiment. The elimination of nitrogen and oxygen from palmitic amide can be seen on Fig. 11a and 11b.

Removal of nitrogen from palmitic amine is effective at high temperature due to high activation energy of denitrogenation ($Ea_{18} = 163$ kJ mol^{-1}). At holding time of 0.37 g_{cat} h g_{amine}^{-1} or 120 min on Fig. 11c the elimination of N corresponds to 35.76 % which is for around 10 % less than results of Verkama et al. (catalyst Ru/ZrO_2, 300 °C, 80 bar H_2) [38]. Ru catalysts produce more pentadecane relying on different mechanisms than NiMoS which produces hexadecane as the main

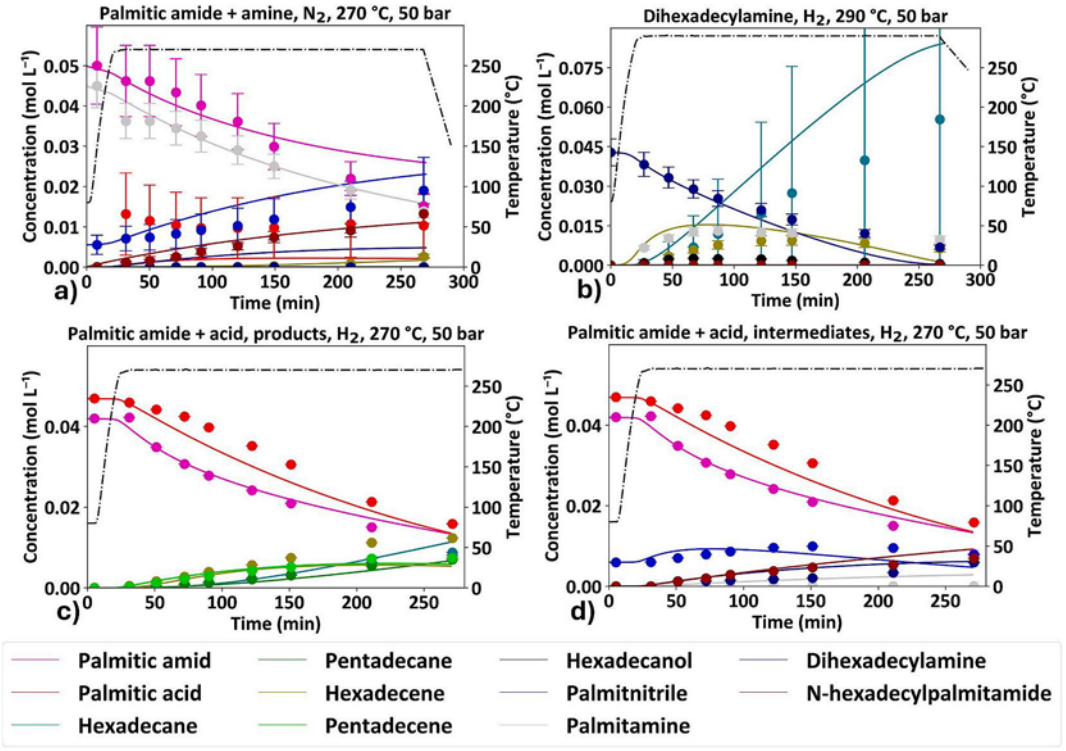

Fig. 10. Reaction with equimolar concentration of palmitic amide and amine (a), dihexadecylamine as model compound (b) and reaction with palmitic amide and acid (c, d).

Table 6
Calculated mass transport criteria.

Resistance	Value
Ca	1.36×10^{-6}
MK	4.71×10^{-5}
N_{W-P}	1.07×10^{-3}

product. Observing the results on Fig. 8, *N*–hexadecylpalmitamide seems to be especially hard to defunctionalize. Additionally, we have in unrelated work calculated the adsorption energies of different functionalities to the sulfided NiMo catalyst edges, and the results show that the alkenes have a very high affinity for these catalytic sites, following the explanation of Prins [39] that the NiMoS catalysts have two types of active sites – for hydrogenolysis and for hydrogenation it might be plausible that the nitrogen species partially deactivate hydrogenation sites while the alkene species reduce the activity of hydrogenolysis sites resulting on overall reduced activity as these species accumulate. The observation needs more theoretical calculations to support it but the reduced activity of palmitic acid HDO in the presence of palmitic amide (Fig. 10) – which would be fully deoxygenated at the same conditions at twice the concentration in absence of palmitic amide shows that the presence of nitrogen species affects the HDO rates very negatively. While the NiMoS catalysts are usually simplified to the activity of the promoted MoS_x edges [36,51] the reality is that the entire catalyst includes catalytic properties. The activity of MoS_x defects was previously showcased by Liu et. al. [52]. The activity of the support for the fatty alcohol dehydration was shown by the Lee et. al. [53] while the activity of the lone Ni sites was shown by the Jeništova et. al. [31]. The complexity of the $NiMoS_x/Al_2O_3$ catalyst is thus reduced to somewhat arbitrary number of active sites.

4.9. Model prediction on the impact of initial feedstock concentrations

The model predicts faster transformation of fatty acid with fatty amide concentrations eventually lowering the yield of alkane products (Fig. 12, left). The impact of smaller molecules on yield is shown on Fig. 12 right, it's clear that water pushes the equilibrium towards more reactive oxygenate reactants while the ammonia lowers the yield by pushing the equilibrium towards nitrogen compounds. The water can to some extent lower the impact of ammonia but does not have a profound effect on the yield. At very high initial concentrations ammonia and water are expected to poison the active sites and have a negative effect on the reaction rate. The effect was observed experimentally at very high water loadings used for the creation of Fig. 6.

4.10. Transport parameters

The Carberry number, Mears's coefficient, and Weisz-Prater criteria were calculated (Table 7) to obtain the importance of transport parameters. All of them were much lower than the limitation values, therefore we concluded that the transport of compounds is not a limitation step but rather a chemical reaction or adsorption or desorption. The calculated coefficient k_L is close to the fitted k_L value indicating the correct presumed H_2 gas–liquid mass transport. Liquid-to-surface transport k_C is much higher than k_L so transport to the surface is a faster process than the solubility of hydrogen in dodecane. Neglection of the liquid–to–surface transport agrees with the literature [27,32,33,54–56]. The results are presented in Table 7.

Additionally, the effectiveness factor was calculated for the highest reactions rates, to show there is no inner resistance. For particles smaller than 100 μm the values are all close to 1. Since we used particles smaller than 100 μm, with average size of ~ 20 μm, so pore impact can be negligible. The Fig. 13 shows calculated effectiveness factor dependant to particle size.

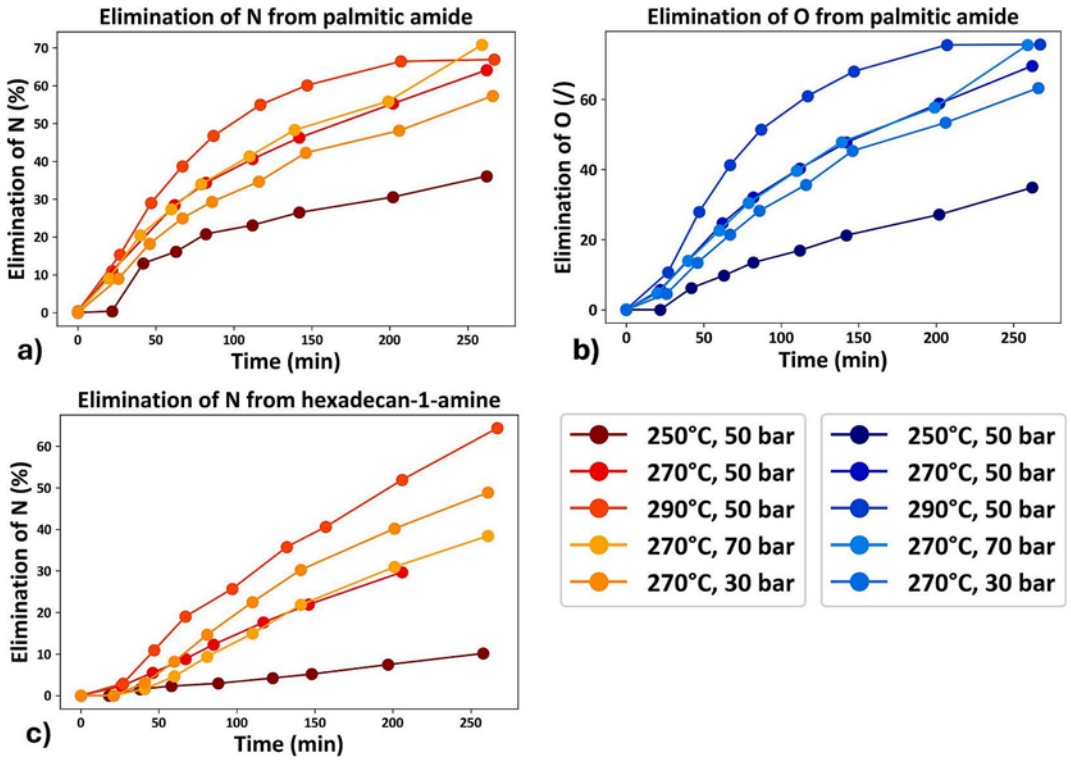

Fig. 11. Elimination on nitrogen and oxygen from palmitic amide (a and b) and palmitic amine (c).

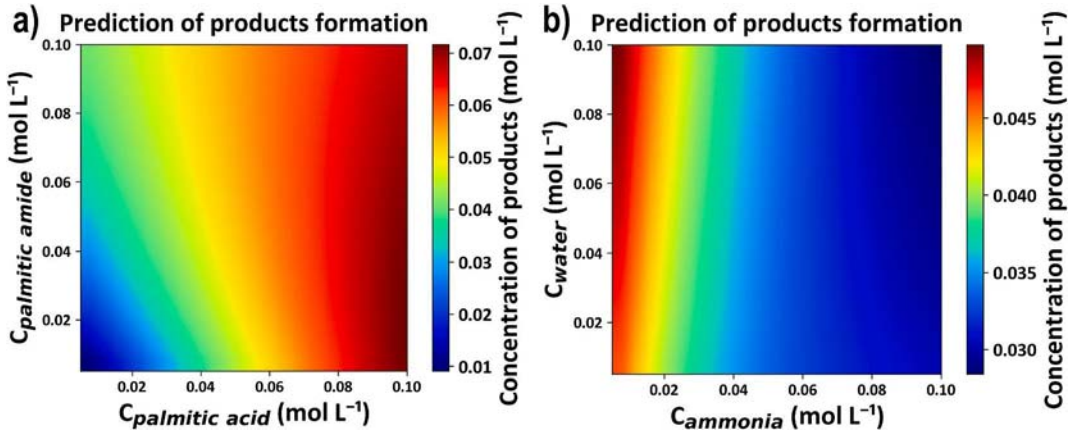

Fig. 12. The model prediction of alkane and alkene products concentration based on initial concentrations at 290 °C for 4 h without the heat-up period at 0.25 g catalyst and 50 bar hydrogen pressure.

Table 7
Results of mass transport parameters.

Parameters of mass transport			
Parameter	Value	Unit	Description
k_L	2.54×10^{-5}	m s^{-1}	Calculated
k_L	2.84×10^{-5}	m s^{-1}	Fitted
k_c	0.201	m s^{-1}	Calculated
a	0.0029	m^2	Interphase area
k_{ads}	$>1.0 \times 10^3$	min^{-1}	Adsorption constant
k_{des}	4.0×10^4	min^{-1}	Desorption constant
k_{ads} (H_2)	14.21	L^2 min^{-1} g_{cat}^{-1}	Adsorption constant for hydrogen
k_{des} (H_2)	1.56×10^4	L^2 min^{-1} g_{cat}^{-1}	Desorption constant for hydrogen

5. Conclusions

We present the model to describe mass transport and the kinetics of hydrodenitrogenation of palmitic amide reactions. The standard hydrotreating catalyst $NiMoS_x/Al_2O_3$ was used to show the mechanism of Nitrogen removal from linear hydrocarbons which are largely present in bio-oil feedstocks. 25 experiments were carried using variety of conditions, i.e. under different temperatures (250–290 °C), pressure (30–70 bar), atmosphere (N_2 and H_2), without and with catalyst (250 mg), and moreover by performing reactions with multiple different starting compounds. Overall, the reaction scheme was formed with 23 chemical reactions, 11 different compounds which reacted over 8 different mechanisms. The model describes the behaviour of 4 different model compounds and their combinations at selected conditions. It elucidates the importance of the equilibrium between fatty amides, free fatty acids, water and ammonia. Our model suggests that the addition of

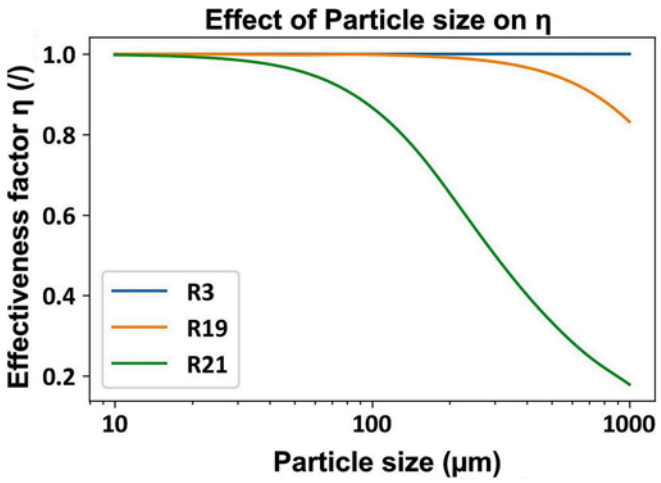

Fig. 13. Effect particle size on inner diffusion.

excess water can translate the reaction pathway from the HDN to the HDO. Additionally, it elucidates the conditions required for the formation of dimers as well as the dependence of reaction occurrence on the presence of H_2. The results are supported with detailed catalyst characterization. The 66.9 % nitrogen removal was achieved with the rest being trapped in recalcitrant dimers which seem harder to defunctionalize. Overall, the work represents the first quantitative description of the hydrotreatment of fatty amides that are often present in lipid-rich biomass. The results clearly show that the presence of nitrogen species significantly reduces the rate of HDO. The mechanism of such reduction in rate is not obvious from the results and needs further study but might be due to hydrogenation sites poisoning or higher binding energy of nitrogen species preventing adsorption of oxygenated species. The results of this study are useful for prediction, comparison and investigation of information obtained from the hydrotreatment of real feedstocks and the prediction and description of catalyst properties – activity relationships for the amide to amine transformations.

CRediT authorship contribution statement

Matej Žula: Writing – review & editing, Writing – original draft, Visualization, Validation, Supervision, Resources, Methodology, Investigation, Formal analysis, Data curation. **Vid Bačar:** Visualization, Validation, Software, Investigation, Formal analysis, Data curation. **Michal Mazur:** Writing – review & editing, Writing – original draft, Methodology, Investigation, Formal analysis, Data curation. **Blaž Likozar:** Writing – review & editing, Supervision, Resources, Project administration, Conceptualization.

Declaration of competing interest

The authors declare that they have no known competing financial interests or personal relationships that could have appeared to influence the work reported in this paper.

Acknowledgements

M.Ž. and B.L. appreciate the funding from the Slovenian Research and Innovation Agency(ARIS) through core funding P2-0152, programme HyBreed and project NC-OO13. MM acknowledges the Czech Science Foundation for the project no. 23-08031 K and OP VVV "Excellent Research Teams" for the project no. CZ.02.1.01/0.0/0.0/15 003/0000417 - CUCAM.

Appendix A. Supplementary data

Supplementary data to this article can be found online at https://doi.org/10.1016/j.cej.2025.162112.

Data availability

Data will be made available on request.

References

[1] P. Cavelius, S. Engelhart-Straub, N. Mehlmer, J. Lercher, D. Awad, T. Brück, The potential of biofuels from first to fourth generation, PLoS Biol. 21 (2023) e3002063, https://doi.org/10.1371/JOURNAL.PBIO.3002063.
[2] F. Johnsson, J. Kjärstad, J. Rootzén, The threat to climate change mitigation posed by the abundance of fossil fuels, Https://Doi.Org/10.1080/14693062.2018.1483885 19 (2018) 258–274. https://doi.org/10.1080/14693062.2018.1483885.
[3] B. Patel, P. Arcelus-Arrillaga, A. Izadpanah, K. Hellgardt, Catalytic hydrotreatment of algal biocrude from fast hydrothermal liquefaction, Renew. Energy 101 (2017) 1094–1101, https://doi.org/10.1016/j.renene.2016.09.056.
[4] C. Yang, R. Li, C. Cui, S. Liu, Q. Qiu, Y. Ding, Y. Wu, B. Zhang, Catalytic hydroprocessing of microalgae-derived biofuels: A review, Green Chem. 18 (2016) 3684–3699, https://doi.org/10.1039/c6gc01239f.
[5] J. Coetzee, D.L. Dodds, J. Klankermayer, S. Brosinski, W. Leitner, A.M.Z. Slawin, D. J. Cole-Hamilton, Homogeneous catalytic hydrogenation of amides to amines, Chem. A Eur. J. 19 (2013) 11039–11050, https://doi.org/10.1002/chem.201204270.
[6] J.R. Cabrero-Antonino, R. Adam, V. Papa, M. Beller, Homogeneous and heterogeneous catalytic reduction of amides and related compounds using molecular hydrogen, Nat. Commun. 11 (2020), https://doi.org/10.1038/s41467-020-17588-5.
[7] H. Yang, L. Zhou, H. Chen, Y. Zeng, D. Li, C. Hu, Efficient hydrogenation of aliphatic acyclic amides to amines by bimetallic NiMo nitrides via heterogeneous catalysis, Chem. Eng. J. 473 (2023), https://doi.org/10.1016/j.cej.2023.145374.
[8] M. Stein, B. Breit, Catalytic hydrogenation of amides to amines under mild conditions, Angew. Chem. 125 (2013) 2287–2290, https://doi.org/10.1002/ange.201207803.
[9] K.I. Shimizu, W. Onodera, A.S. Touchy, S.M.A.H. Siddiki, T. Toyao, K. Kon, Lewis acid-promoted heterogeneous platinum catalysts for hydrogenation of amides to amines, ChemistrySelect 1 (2016) 736–740, https://doi.org/10.1002/slct.201600088.
[10] T. Toyao, S.M.A.H. Siddiki, Y. Morita, T. Kamachi, A.S. Touchy, W. Onodera, K. Kon, S. Furukawa, H. Ariga, K. Asakura, K. Yoshizawa, K.I. Shimizu, Rhenium-loaded TiO2: A highly versatile and chemoselective catalyst for the hydrogenation of carboxylic acid derivatives and the N-methylation of amines using H2 and CO2, Chem. A Eur. J. 23 (2017) 14848–14859, https://doi.org/10.1002/chem.201702801.
[11] M. Cattenot, E. Peeters, C. Geantet, E. Devers, J.L. Zotin, Mechanism of carbon-nitrogen bond scission in the presence of H 2S on Pt Supported catalysts, Catal. Lett. 99 (2005) 171–176, https://doi.org/10.1007/s10562-005-2110-z.
[12] G. Beamson, A.J. Papworth, C. Philipps, A.M. Smith, R. Whyman, Selective hydrogenation of amides using ruthenium/ molybdenum catalysts, Adv. Synth. Catal. 352 (2010) 869–883, https://doi.org/10.1002/adsc.200900824.
[13] T. Mitsudome, K. Miyagawa, Z. Maeno, T. Mizugaki, K. Jitsukawa, J. Yamasaki, Y. Kitagawa, K. Kaneda, Mild Hydrogenation of Amides to Amines over a Platinum-Vanadium Bimetallic Catalyst, Angewandte Chemie - International Edition 56 (2017) 9381–9385, https://doi.org/10.1002/anie.201704199.
[14] S. Chakraborty, H. Berke, Homogeneous hydrogenation of nitriles catalyzed by molybdenum and tungsten amides, ACS Catal. 4 (2014) 2191–2194, https://doi.org/10.1021/cs5004646.
[15] F. Yaşar, Comparision of fuel properties of biodiesel fuels produced from different oils to determine the most suitable feedstock type, Fuel 264 (2020) 116817, https://doi.org/10.1016/J.FUEL.2019.116817.
[16] (PDF) Palm biodiesel an alternative green renewable energy for the energy demands of the future, (n.d.). https://www.researchgate.net/publication/284892057_Palm_biodiesel_an_alternative_green_renewable_energy_for_the_energy_demands_of_the_future (accessed September 7, 2023).
[17] G.M. Figueroa-Torres, C. Theodoropoulos, Techno-economic analysis of a microalgae-based biorefinery network for biofuels and value-added products, Bioresour. Technol. Rep. 23 (2023), https://doi.org/10.1016/j.biteb.2023.101524.
[18] M. Wiatrowski, B.C. Klein, R.W. Davis, C. Quiroz-Arita, E.C.D. Tan, R.W. Hunt, R. E. Davis, Techno-economic assessment for the production of algal fuels and value-added products: opportunities for high-protein microalgae conversion, Biotechnol. Biofuels Bioproducts 15 (2022), https://doi.org/10.1186/s13068-021-02098-3.
[19] T. Ročnik Kozmelj, M. Žula, J. Teržan, B. Likozar, U. Maver, L. Činč Ćurić, E. Jasiukaitytė-Grojzdek, M. Grilc, Understanding stability, oligomerization and deactivation during catalytic lignin hydrodeoxygenation by mechanistic reaction micro-kinetics linked with 3D catalyst particle nanotomography, J. Clean Prod. 414 (2023), https://doi.org/10.1016/j.jclepro.2023.137701.
[20] T.H. Kim, K. Lee, M.Y. Kim, Y.K. Chang, M. Choi, Effects of fatty acid compositions on heavy oligomer formation and catalyst deactivation during deoxygenation of

triglycerides, ACS Sustain. Chem. Eng. 6 (2018) 17168–17177, https://doi.org/10.1021/acssuschemeng.8b04552.
[21] P. Arora, H. Ojagh, J. Woo, E. Lind Grennfelt, L. Olsson, D. Creaser, Investigating the effect of Fe as a poison for catalytic HDO over sulfided NiMo alumina catalysts, Appl. Catal. B 227 (2018) 240–251, https://doi.org/10.1016/j.apcatb.2018.01.027.
[22] M.A. Salam, D. Creaser, P. Arora, S. Tamm, E.L. Grennfelt, L. Olsson, Influence of bio-oil phospholipid on the hydrodeoxygenation activity of NiMoS/Al2O3 catalyst, Catalysts 8 (2018), https://doi.org/10.3390/catal8100418.
[23] P. Arora, H. Abdolahi, Y.W. Cheah, M.A. Salam, E.L. Grennfelt, H. Rådberg, D. Creaser, L. Olsson, The role of catalyst poisons during hydrodeoxygenation of renewable oils, Catal. Today (2020), https://doi.org/10.1016/j.cattod.2020.10.026.
[24] D. Castello, M.S. Haider, L.A. Rosendahl, Catalytic upgrading of hydrothermal liquefaction biocrudes: Different challenges for different feedstocks, Renew. Energy 141 (2019) 420–430, https://doi.org/10.1016/J.RENENE.2019.04.003.
[25] R. Prins, Catalytic hydrodenitrogenation, Adv. Catal. 46 (2001) 399–464, https://doi.org/10.1016/S0360-0564(02)46025-7.
[26] J.E. Davis, Preparation of amides of higher fatty acids, US Patents (1962).
[27] M. Žula, M. Grilc, B. Likozar, Mechanistic reaction micro-kinetics-based structure–activity relationships for palmitic acid hydrodeoxygenation over NiMoSx/Al2O3 catalysts, Chem. Eng. J. 467 (2023) 143425, https://doi.org/10.1016/J.CEJ.2023.143425.
[28] M. Grilc, B. Likozar, Levulinic acid hydrodeoxygenation, decarboxylation and oligmerization over NiMo/Al2O3 catalyst to bio-based value-added chemicals: Modelling of mass transfer, thermodynamics and micro-kinetics, Chem. Eng. J. 330 (2017) 383–397, https://doi.org/10.1016/J.CEJ.2017.07.145.
[29] M. Žula, M. Grilc, B. Likozar, Hydrocracking, hydrogenation and hydrodeoxygenation of fatty acids, esters and glycerides: Mechanisms, kinetics and transport phenomena, Chem. Eng. J. 444 (2022), https://doi.org/10.1016/j.cej.2022.136564.
[30] P. Arora, E.L. Grennfelt, L. Olsson, D. Creaser, Kinetic study of hydrodeoxygenation of stearic acid as model compound for renewable oils, Chem. Eng. J. 364 (2019) 376–389, https://doi.org/10.1016/j.cej.2019.01.134.
[31] K. Jeništová, I. Hachemi, P. Mäki-Arvela, N. Kumar, M. Peurla, L. Čapek, J. Wärnå, D.Y. Murzin, Hydrodeoxygenation of stearic acid and tall oil fatty acids over Ni-alumina catalysts: Influence of reaction parameters and kinetic modelling, Chem. Eng. J. 316 (2017) 401–409, https://doi.org/10.1016/j.cej.2017.01.117.
[32] A.A. Michael, A. Matthews, J.B. Rodden, High-temperature diffusion of hydrogen, carbon monoxide, and carbon dioxide in liquid n-heptane, n-dodecane, and n-hexadecane, J. Chem. Eng. Data (1987) 319–322.
[33] T.M. Koller, T. Klein, C. Giraudet, J. Chen, A. Kalantar, G.P. Van Der Laan, M. H. Rausch, A.P. Fröba, Liquid viscosity and surface tension of n-dodecane, n-octacosane, their mixtures, and a wax between 323 and 573 K by surface light scattering, J. Chem. Eng. Data 62 (2017) 3319–3333, https://doi.org/10.1021/acs.jced.7b00363.
[34] J.I. del Río, F. Cardeño, W. Pérez, J.D. Peña, L.A. Rios, Catalytic hydrotreating of jatropha oil into non-isomerized renewable diesel: Effect of catalyst type and process conditions, Chem. Eng. J. 352 (2018) 232–240, https://doi.org/10.1016/j.cej.2018.07.021.
[35] X. Wang, Z. Zhao, P. Zheng, Z. Chen, A. Duan, C. Xu, J. Jiao, H. Zhang, Z. Cao, B. Ge, Synthesis of NiMo catalysts supported on mesoporous Al2O3 with different crystal forms and superior catalytic performance for the hydrodesulfurization of dibenzothiophene and 4,6-dimethyldibenzothiophene, J. Catal. 344 (2016) 680–691, https://doi.org/10.1016/J.JCAT.2016.10.016.
[36] M. Žula, M. Grilc, B. Likozar, Mechanistic reaction micro-kinetics-based structure–activity relationships for palmitic acid hydrodeoxygenation over NiMoSx/Al2O3 catalysts, Chem. Eng. J. 467 (2023), https://doi.org/10.1016/j.cej.2023.143425.
[37] M.F. Wagenhofer, E. Baráth, O.Y. Gutiérrez, J.A. Lercher, Carbon-carbon bond scission pathways in the deoxygenation of fatty acids on transition-metal sulfides, ACS Catal. 7 (2017) 1068–1076, https://doi.org/10.1021/acscatal.6b02753.
[38] E. Verkama, P. Auvinen, S. Albersberger, M. Tiitta, R. Karinen, R.L. Puurunen, Competitive hydrodeoxygenation and hydrodenitrogenation reactions in the hydrotreatment of fatty acid and amine mixtures, Top. Catal. 66 (2023) 1353–1368, https://doi.org/10.1007/S11244-023-01784-W/FIGURES/7.
[39] R. Prins, Catalytic hydrodenitrogenation, Adv. Catal. 46 (2001).
[40] A.K. Ravn, N.M. Rezayee, The investigation of a switchable iridium catalyst for the hydrogenation of amides: a case study of C-O versus C-N bond scission, ACS Catal. 12 (2022) 11927–11933, https://doi.org/10.1021/acscatal.2c03247.
[41] D. Kumar, C.H. Park, C.S. Kim, Sustainable heterogeneously catalyzed single-step and two-step amide derivatives of non-edible natural triglycerides as dual-functional diesel fuel additives, Ind. Crop. Prod. 158 (2020), https://doi.org/10.1016/j.indcrop.2020.113001.
[42] L. Matricon, A. Roubaud, G. Haarlemmer, C. Geantet, The challenge of nitrogen compounds in hydrothermal liquefaction of algae, J. Supercrit. Fluids 196 (2023), https://doi.org/10.1016/j.supflu.2023.105867.
[43] J. Watson, M. Swoboda, A. Aierzhati, T. Wang, B. Si, Y. Zhang, Biocrude oil from algal bloom microalgae: a novel integration of biological and thermochemical techniques, Environ. Sci. Tech. 55 (2021) 1973–1983, https://doi.org/10.1021/acs.est.0c05924.
[44] E. Verkama, S. Albersberger, K. Meinander, M. Tiitta, R. Karinen, R.L. Puurunen, Zirconia-supported Pt, Pd, Rh, Ru, and Ni catalysts in the hydrotreatment of fatty amides and amines, Energy Fuel 38 (2024) 4464–4479, https://doi.org/10.1021/ACS.ENERGYFUELS.3C04372/ASSET/IMAGES/LARGE/EF3C04372_0008.JPEG.
[45] M.T. Nguyen, M. Tayakout-Fayolle, F. Chainet, G.D. Pirngruber, C. Geantet, Use of kinetic modeling for investigating support acidity effects of NiMo sulfide catalysts on quinoline hydrodenitrogenation, Appl. Catal. A 530 (2017) 132–144, https://doi.org/10.1016/j.apcata.2016.11.015.
[46] M.T. Nguyen, M. Tayakout-Fayolle, G.D. Pirngruber, F. Chainet, C. Geantet, Kinetic modeling of quinoline hydrodenitrogenation over a NiMo(P)/Al2O3 catalyst in a batch reactor, Ind. Eng. Chem. Res. 54 (2015) 9278–9288, https://doi.org/10.1021/acs.iecr.5b02175.
[47] C. Zhu, O.Y. Gutiérrez, D.M. Santosa, M. Flake, R. Weindl, I. Kutnyakov, H. Shi, H. Wang, Kinetics of nitrogen-, oxygen- and sulfur-containing compounds hydrotreating during co-processing of bio-crude with petroleum stream, Appl. Cataly. B: Environ. Energy 307 (2022) 121197, https://doi.org/10.1016/J.APCATB.2022.121197.
[48] E. Verkama, S. Albersberger, A. Arandia, K. Meinander, M. Tiitta, R. Karinen, R. L. Puurunen, Hydrodeoxygenation and hydrodenitrogenation of n -hexadecanamide over Pt catalysts: effect of the support, Catal, Sci. Technol. 14 (2024) 431–448, https://doi.org/10.1039/D3CY01480K.
[49] R. Shakya, S. Adhikari, R. Mahadevan, E.B. Hassan, T.A. Dempster, Catalytic upgrading of bio-oil produced from hydrothermal liquefaction of Nannochloropsis sp, Bioresour. Technol. 252 (2018) 28–36, https://doi.org/10.1016/J.BIORTECH.2017.12.067.
[50] M.S. Haider, D. Castello, L.A. Rosendahl, Two-stage catalytic hydrotreatment of highly nitrogenous biocrude from continuous hydrothermal liquefaction: A rational design of the stabilization stage, Biomass Bioenergy 139 (2020) 105658, https://doi.org/10.1016/J.BIOMBIOE.2020.105658.
[51] C. Dupont, R. Lemeur, A. Daudin, P. Raybaud, Hydrodeoxygenation pathways catalyzed by MoS2 and NiMoS active phases: A DFT study, J. Catal. 279 (2011) 276–286, https://doi.org/10.1016/j.jcat.2011.01.025.
[52] G. Liu, A.W. Robertson, M.M.J. Li, W.C.H. Kuo, M.T. Darby, M.H. Muhieddine, Y. C. Lin, K. Suenaga, M. Stamatakis, J.H. Warner, S.C.E. Tsang, MoS2 monolayer catalyst doped with isolated Co atoms for the hydrodeoxygenation reaction, Nat. Chem. 9 (2017) 810–816, https://doi.org/10.1038/NCHEM.2740.
[53] H.J. Lee, I.H. Choi, S.W. Kim, K.R. Hwang, Selective production of bio-based linear alpha-olefin from wasted fatty alcohol on al2o3 for bio-based chemicals, Polymers (Basel) 13 (2021), https://doi.org/10.3390/polym13172850.
[54] J. Lourenço Castagnari Willimann Pimenta, M. Oliveira Camargo, R. Belo Duarte, O. Aparecida Andreo Santos, L. Mario Matos Jorge, A novel kinetic model applied to heterogeneous fatty acid deoxygenation, Chem. Eng. Sci. 230 (2021) 116192, https://doi.org/10.1016/j.ces.2020.116192.
[55] R. V Chaudhari, R. V Gholap, G. Emlg, H. Hofmann, Gas-Liquid Mass Transfer in ' ' Dead-End'' Autoclave Reactors, n.d.
[56] W. Gao, R.L. Robinson, K.A.M. Gasem, High-pressure solubilities of hydrogen, nitrogen, and carbon monoxide in dodecane from 344 to 410 K at pressures to 13.2 MPa, J. Chem. Eng. Data 44 (1999) 130–132, https://doi.org/10.1021/je9801664.